VIBRO-ACOUSTIC MODULATION MEASUREMENTS FOR A LIFETIME EVALUATION OF COMPOSITE MATERIALS

E. Willmann[1*], B. Boll[1,2], M. Scheel[1] ,T. Dräger[2], R. Meißner[1,2], B. Fiedler[1]
[1] Institute of Polymers and Composites, TU Hamburg, Germany
[2] Institute of Surface Science, Helmholtz-Center Hereon, Geesthacht, Germany
* Corresponding author (erik.willmann@tuhh.de)

Keywords: Fiber reinforced composites, Health monitoring, Non-destructive testing, Vibro-acoustic modulation, Damage progression

ABSTRACT

This paper investigates the influence of different damage types and their interaction on the vibro-acoustic behaviour of glass fibre and carbon fibre reinforced polymers (GFRP and CFRP) under step-wise tensile and fatigue loading. For this purpose, different GFRP layups were used to correlate visible matrix cracks with VAM signal. Additionally, for CFRP the layer thicknesses are varied for cross-ply laminates with constant areal fibre weight (268 g/m^2) and quasi-isotropic laminates with different areal fibre weights (30, 60 and 120 g/m^2). After damage introduction under tension-tension loading (R=0.1), high-frequency Lamb waves are introduced via bonded piezo ceramic actuator and modulated by a low-frequency longitudinal wave using a servo-hydraulic testing machine. In this study, the analysis and interpretation of the vibro-acoustic response signal can be used to demonstrably identify different damage types and conditions of the CFRP specimens. The sideband amplitudes and the modulation index are used as VAM characteristics in the frequency domain and the shape of the modulation envelope in time domain as well as X-ray scans to prove the damage progress after various cycles. It is shown that regardless of the lay-up, both inter-fibre failures, as well as extensive delaminations, can be reliably and sensitively detected using a simple vibration-based test setup, providing a promising non-destructive testing methodology. Finally, it is demonstrated that for certain GFRP specimens the modulation index and lifetime can be predicted after only a few loading cycles.

1 INTRODUCTION

Fibre-reinforced polymers (FRP) are used in numerous lightweight structures in aerospace, automotive or sports equipment, where high specific strength and stiffness as well as high fatigue resistance are essential. Due to their multi-layer structure and their various constituents, the failure behavior of composites is, however, very complex. Composites are generally characterized by brittle behavior, where fatigue loads can lead to sudden failure. Due to their specific failure mechanisms-including matrix cracking, delamination, and fiber breakage - the stiffness and strength of composites decrease under fatigue loading. Matrix cracks developing at low stress lead to delamination with increasing crack length and the associated stress maxima at the crack tip, resulting in a significant decrease in stiffness during fatigue [1–3]. The failure mechanisms of FRP are strongly dependent on the layer thickness. A lower layer thickness suppresses microcrack initiation in the transverse direction and edge delamination, which leads to increased transverse tensile strength (in-situ effect) [4]. Reducing the layer thickness changes the failure mode from a complex failure dominated by delamination to a brittle failure [4-8].

Structural health monitoring (SHM) that reliably detects this complex damage behaviour in-situ at an early stage, before a composite component is subjected to failure-critical loads, is consequently necessary. Ideally, structural safety is significantly increased, and inspection costs, as well as machine down-times are reduced. Most non-destructive testing (NDT) methods have a supporting effect during certain maintenance intervals of the component, e.g. ultrasonic inspection or x-ray examination, but detect the damage late, when it is already pronounced. These methods capable of detecting damages are localised methods, which makes them expensive and time-consuming and underlining the need for a global active SHM method [9]. SHM approaches like the Lamb wave method gained attention due to its low operating cost, high sensitivity, and long propagation distances [10].

A very promising NDT method, sensitive to damages and other material non-linearities is the vibro-acoustic modulation (VAM) method. It combines the benefits of a high-frequency lamb-wave as sensing wave with a low-frequency structural wave to periodically change the stress state around damages in the material which results in a non-linear modulated signal. The high sensitivity in fatigue damage detection of metals and impact detection of composites has already been demonstrated [11–16]. However, a systematic change of the laminate structure of FRP to show the influence of composite typical damage types to the vibro-acoustic signal is missing in literature. This approach is intended contributes to the understanding of the vibro-acoustic signal in composite materials.
For this purpose, the primary aim of this study is to correlate the damage development of composites under fatigue loading with VAM and to investigate characteristic curves of the response signal. Decicated to this purpose, the influence of crack size and crack density on the vibro-acoustic modulation is investigated with regard to the variation of the single layer thickness. GFRP laminates are subjected to stepwise and cyclic tensile tests (R=0.1) for this purpose. CFRP laminates, on the other hand, are tested under tensile fatigue load to introduce damages, followed by the vibro-acoustic measurement is carried out via high-frequency vibrations through a piezoceramic and low-frequency vibrations using a servo-hydraulic testing machine. X-Ray scans are used to detect the type and severity of the damage.

2 MATERIALS AND METHODS

Vibro-acoustic Modulation

This VAM measurement is performed by the simultaneous excitation of a high-frequency ultrasonic probe wave (f_{Ca}) and a low-frequency pump vibration (f_P). The pump vibration changes the stress state in the specimen and therefore modulates the propagation of the probe wave [17]. Figure 1 illustrates the principles of VAM and the influence of inhomogeneities in the time and frequency domain. In the time domain, this leads to frequency modulation (FM) and amplitude modulation (AM) of the probe wave with a high and pronounced envelope due to the pump oscillation. The more inhomogeneities (e.g. defects, phase transitions) occur in the material or are introduced by continuous loading, the stronger the degree of modulation, whether in the form of frequency or amplitude [18]. A strong modulation leads to sidebands with high amplitudes in the frequency range. Amplitude-only modulation ideally results in one positive and one negative sideband ($f_{Ca} \pm f_P$), while frequency modulation does not limit the number of sidebands ($f_{Ca} \pm n \cdot f_P$) [19,20]. The measured signal contains both AM and FM. The phase modulation can be partially extracted from the signal by the short-time Fourier transform [19]. To be able to analyse the measured signal, different damage indices are usually used. A frequently used damage index is the modulation index [11,15] (MI), which is given in equation (1) as the ratio between the amplitude of the sideband components and the amplitude of the carrier frequency. It is often observed that an increasing number of inhomogeneities, such as cracks or delaminations, increases the MI [11,21,22].

$$MI = 20 \cdot log_{10}\left(\frac{A_{1+} + A_{1-}}{2 \cdot A_C}\right) \quad (1)$$

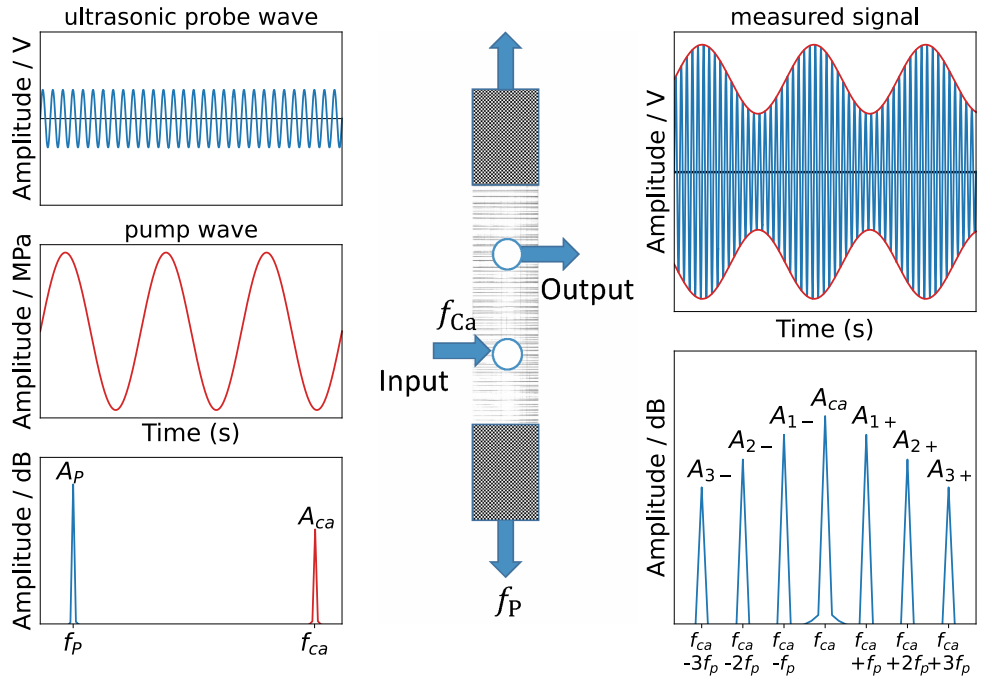

Figure 1: Illustration of the VAM principle. Due to damages and inhomogeneities in the FRP the output signal is modulated.

Materials and specimen preparation

In this study GFRP and CFRP laminates were used. Within the RTM-process unidirectional fibres UT-E500 from Gurlit and +-45° biaxial G300BX-1270 from Hacotec were injected by the low-viscosity resin system EPIKOTE™ Resin MGS® RIM 135 with EPIKURE™ Curing Agent MGS® RIMH 137, commonly used in the wind energy industry. These different layer structures were fabricated with a thickness of 3 mm and a resulting fibre volume ratio of apox. 50%. To investigate whether the formation of cracks in the matrix under tensile stress and their evolution can be identified and detected with VAM, a cross-ply $[0/90_3]_s$ structure with unidirectional fibres was chosen. An $[0/\pm45_4]$s lay-up was used to investigate matrix damage initiation under shear loading.

Two different CFRP prepreg systems were used in this study, illustrated in Table 1 including layup and GFRP material. Hexcel's HexPly M21/35/268/T800S prepreg system was used to investigate the vibro-acoustic response signals of unidirectional manufactured aerospace laminates. Quasi-isotropic (QI) samples with low fibre basis weights (30 g/m^2, 60 g/m^2 and 120 g/m^2) were fabricated using NTPT ThinPreg 402 epoxy resin from North Thin Ply Technology (NTPT), Switzerland, and Toray T700SC-12K-60E fibres from Toray Industries, Japan. For comparison with higher fibre basis weights, the HexPly prepreg system with 268 g/m^2 was also used for QI samples.

A CNC cutter (Aristomat TL1625 from ARISTO Graphic Systeme GmbH & Co. KG i.I., Germany) was used to shape and manually laminate these prepreg layers. During laminating, an intermediate vacuum was applied at every fourth layer in the stacking sequence to compress the layers and prevent air pockets. Curing was carried out in an autoclave process. Specific curing parameters were used according to the manufacturer's recommendations. Thick film prepregs were cured at 180°C for 4 h with a pressure of 7 bar. Thin film prepregs were cured at 160°C for 4 h, also with a pressure of 7 bar. To reduce the stress concentration in the load application area and thus prevent premature failure under fatigue loading, GFRP with a ±45° layup and aluminium tabs, each 1 mm thick, were bonded to the CFRP specimen. These tabs cover 50 mm of both ends of the specimen and were bonded with UHU Endfest Plus 300, which was cured at 80°C. All laminates were cut with a diamond cutting wheel on a high precision saw (ATM Brillant 265 from QATM, Germany) to the dimensions according to ASTM tensile standard (ASTM D3039-00) [23], which are listed in *Table 2*.

Table 1: Laminate layups of used CFRP and GFRP laminates.

Composite Material	Areal Weight in g/m^2	Layup
Hexion RIMR135+RIMH137 +glass-fibres	500 (Gurlit UT-E500) 300 (Hacotec G300BX-1270)	$[0/90_3]_s$ $[0/\pm45_4]s$
HexPly M21+T800s	268	CP: $[0/90_7]_s$ CP: $[0/90_6/0]_s$ CP: $[0/90]_{4s}$ QI: $[0/90_7]_s$
NTPT TP402+T700s	30 60 120	$[45/90/-45/0]_{12s}$ $[45/90/-45/0]_{6s}$ $[45/90/-45/0]_{3s}$

Table 2: Dimensions of tested specimens

Specimen Dimension	RIMR135+RIMH137	HexPly M21+T800s	NTPT TP402+T700s
Overall length in mm	250	250	250
Width in mm	30	20	25
Thickness in mm	3.00	2.88	2.88
Tab length in mm	40	50	50
Free test length in mm	180	150	150

Experimental methods

Quasi-static tensile tests according to ASTM D3039-00 [23] were performed on a universal testing machine (ZwickRoell Z100 with Multi-Xtens for strain recording) to determine the stress values for stepwise-tensile tests and the fatigue stress amplitudes. The step-wise tensile tests and fatigue tests were performed on the servo-hydraulic universal testing machine Instron 8802L2741 to initiate the tensile load and longitudinal pump wave in tension control mode. The pump excitation is generated after each unloading phase of the step-wise tensile test.

Fatigue testing was carried out using the tension-tension regime (stress ratio R=0.1). The ambient conditions were constant with a temperature and relative humidity of 23°C and 50 % respectively. The test procedures and data collection were carried out using WaveMatrix software (Instron).
The vibro-acoustic measurements were performed similarly to [17,24,25]. For each specimen, a pump amplitude and a fatigue amplitude with the same frequency (3 Hz for CFRP and 5 Hz for GFRP) were introduced.

To avoid damage within the VAM measurement, $\sigma_{A,P} = 31.5$ MPa was chosen as the pump amplitude under tensile-tensile load (R=0.1). Depending on the laminate structure, this pump amplitude corresponds to Piezoceramic actuator discs (PI-Ceramics 10x2 mm) were used to excite the high-frequency signal. The piezoceramic disc bonding were varied by using the epoxy resin system Loctite EA 9455, double-sided adhesive tape (tesa 56172) and hot melt 47872 from UHU. The NI-USB 6366 data acquisition card from National Instruments with a sampling rate of 2 MS/s was used for carrier wave excitation and measurement of the system response. The carrier signal was amplified to 50 V_{PP} by a Falco Systems WMA-300 high voltage amplifier. For the test signal, a linear frequency sweep from 1 to 300 kHz was first performed to select a frequency band (185-230 kHz for CFRP and 190-225 kHz for GFRP with a step size of 1 kHz) where the system response was strongest.

Figure 2 shows schematically the order in which the high and low frequency vibrations are initiated. Typically, matrix cracks of FRP occur more frequently at the beginning of the service life, leading to rapid degradation. In order to detect this stiffness-reducing damage with the help of the VAM, an initial measurement is carried out before the first onset of fatigue. Further VAM measurements at pump

amplitude ($\sigma_{A,P} = 31.5$ MPa) follow in logarithmically increasing number of fatigue cycles after 1, 11, 111 and 1111 fatigue cycles. Subsequent measurements were carried out after 3570 fatigue cycles each, which corresponds to 20 min for CFRP specimens and after 2000 fatigue cycles, which is equivalent to 7 min for GFRP.

Data preparation

A time domain signal generated by the piezo ceramic receiver is stored by a MATLAB script and converted to the frequency domain using the Numpy FFT package in Python 3.7. A Hanning window was used to reduce spectral leakage and achieve high frequency resolution. The carrier and the positive and negative sidebands were searched for as maxima within the respective frequency range for each measured signal. The negative and the positive sidebands were extracted up to the 8th sideband for further evaluation in a Pandas Dataframe.

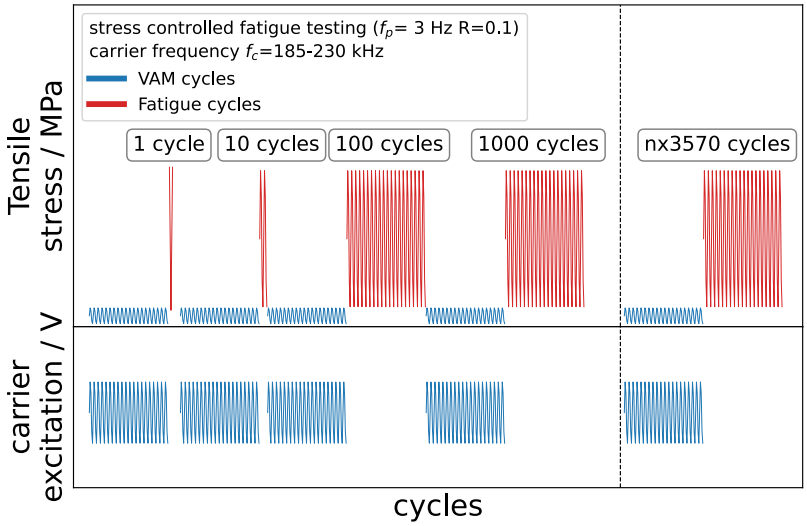

Figure 2:Schematic test procedure for fatigue tests with VAM measurement. First VAM measurement at initial state and after logarithmic increasing number of fatigue cycles, second measurement applied as repeating loops

3 RESULTS

3.1 GFRP

Step-wise-Tensile tests

In preliminary tests, the signal strength of introduced Lamb waves was 35-40% higher when using the Loctite epoxy resin system versus double-sided adhesive tape or hot melt. The influence of the different piezo contacting in VAM measurements is clearly shown in Fig. 3a. The qualitative plots of MI over the number of cracks for GFRP with $[0/90_3]_s$ configuration are very similar. The cracks were visually documented by pictures after each load level and counted afterwards. Thus, the sensitivity in the form of MI increase is the same for all 3 contact types, only the level of MI (respective signal strength) is higher for epoxy bonding with an average of 2.5 dB compared to hot melt bonding and double-sided tape. As with the Lamb wave measurement before, these are in the same magnitude range. Accordingly, the double-sided adhesive tape can even be reused as fixations for the piezo ceramics. Figure 3b shows the comparison between cross-ply laminate ($[0/90_3]_s$) with the biaxial laminate $[0/\pm45_4]_s$ during a step-wise tensile test. Whereas the first cracks in the 90° layers can already be detected optically after 4 kN, resulting in an increase of the MI by 2 dB, the MI of the $[0/\pm45_4]_s$ laminate only increases from 7 kN load. The cracks in the ±45° layers were not clearly visible but resulted in opacity, which is why the number of cracks in the $[0/\pm45_4]_s$ laminate is missing in Fig. 3b. However, it is noticeable that the MI increase is clearly more pronounced for 90° cracks due to larger crack opening and this increases to 34 dB up to 10 kN, whereas for 45° matrix cracks it increases to 6 dB.

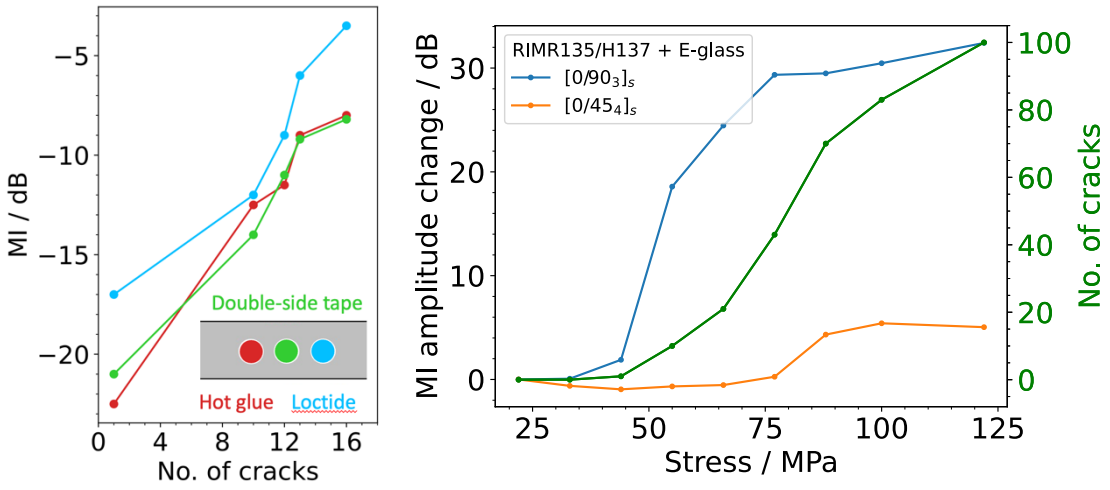

Figure 3:a) Comparison of different piezoceramic disc bonding and b) Correlation between the MI and the number of cracks on GFRP specimens during a step-wise tensile test

Fatigue tests

The fatigue results of a representative GFRP laminate with a $[0/\pm45_4]_s$ layup is shown in Fig 4a. Here, the MI follows the damage curve quite well. Even after the second VAM measurement, which was performed after 10 load cycles, the MI increased by 7.2 dB. Until failure, the MI increases by 13.5 dB. The initial rapid increase correlates well with the staged tensile tests, where initial damage occurs at about 77 MPa. The MI curve correlates very well with the damage curve calculated from the relative stiffness of the laminate, both of which follow a logarithmic function. The approximation of the MI curve using the function f(x)=a·ln(x-b)+c demonstrates a very good agreement. With this approximating function, the averaged parameter a=2.37+-0.17 for $[0/\pm45_4]_s$ laminates. A prediction of MI can already be made with a deviation of 1 dB after 15 measurements, while a 6.8 dB deviation is present after 5 measurements. Failure predictions were determined based on 4 parameters of the measured MI and are shown in Fig.4b. The absolute averaged MI value measured after failure was -28.35 ± 1.8 dB and was calculated to be -29.275 dB by least square error. With an initial high error, it levelizes at about 30,000 cycles, but increases adversely as the life progresses. The MI increase to failure averages -14.98 dB and was calculated to be -14.6 dB using least square error. Compared to the absolute MI value, the prediction error is halved to 15,000 load cycles, but the prediction also deteriorates after about 30% of the life. When deriving the MI after 1000 loading cycles, the average error drops below 20,000 loading cycles after about 20% of the life. As the life progresses, the prediction becomes more accurate, so that the error falls to about 10,000 load cycles. The fourth parameter a of the logarithmic function for the service life prediction has a high error of 40,000 load cycles up to 10% of the service life, but decreases to about 13,000 cycles as the service life progresses.

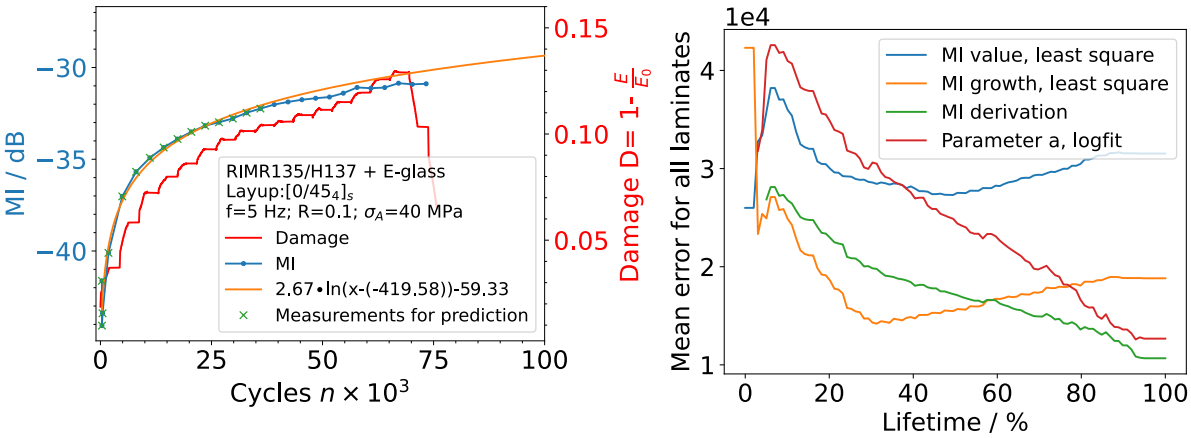

Figure 4: a) Representative results of fatigue tests on GFRP laminates [0/±45$_4$]$_s$ layup, including the MI Amplitude and damage curve and the predicted MI based on 15 preliminary measurements with resulting logarithmic fit equation. b) Comparison of 4 lifetime prediction methods

3.1 CFRP

Fatigue tests of thick-ply laminates [268 g/m^2]

Cross-ply laminates

With the knowledge that in GFRP the matrix cracks can be detected in 90° as well as in 45° layers by using VAM, the influence of crack length and crack density on the VAM signal shall now be investigated. In the following, the amplitude change (from left and right sideband) to the initial measurement for the first eight sidebands are presented for three exemplary CP specimens in Figure 5. The relative specimen stiffness describes the ratio between the stiffness after cycle n and the initial stiffness.

Due to the differences in the layups, the maximal load was adjusted to 65 % of the maximum tensile strength, resulting in fatigue stress amplitudes of $\sigma_{A,F}$ = 187 MPa for [0/90$_7$]$_s$, $\sigma_{A,F}$ = 234 MPa for [0/90$_6$0]$_s$ and $\sigma_{A,F}$= 500 MPa for [0/90]$_{4s}$. These presented specimens were stopped after 34,081 cycles ([0/90$_7$]$_s$), 33,091 cycles ([0/90$_6$0]$_s$) and 166,766 cycles ([0/90]$_{4s}$) and accordingly have not failed.

After the initial loads, the sideband amplitudes of the [0/90$_7$]$_s$ and [0/90$_6$0]$_s$ laminates remain almost constant. The highest increase in sideband amplitude is measured for the [0/90$_7$]$_s$ laminate. However, the second sideband increases from -77 dB by more than twice as much (approx. 31 dB) as the first sideband (12 dB) between the initial and the first measurement after fatigue load. The remaining sidebands show a similar strong increase and a graded, identical curve as the second sideband. This strong increase is in very good agreement with the relative stiffness decrease by more than 20 % (see Figure 5). The measured increase of the higher order sidebands after the first load has a magnitude of 35.4±2.3 dB. A lower increase in the sideband amplitudes after the first load is observed for the [0/90$_6$0]$_s$ samples. The first two sidebands increase by 8.2±1.1 dB and 18.4±1.7 dB respectively, while the increase of the higher sidebands is 22.1±3.8 dB. The measured amplitude change and MI show an excellent agreement with relative stiffness reduction to 10 % (see Figure 5). In contrast, there is no significant increase in the sideband amplitudes and MI for the [0/90]$_{4s}$ laminate as they remain in the same order of magnitude. This correlates well with the small relative stiffness reduction of 2 % after first load cycle. Regarding CP-laminates in general, the cracks in the first cycles have the strongest influence on the sideband amplitudes and the MI. Furthermore, these VAM characteristics remain in the same order of magnitude since crack saturation occurred, which is consistent with a weakly decreasing stiffness.

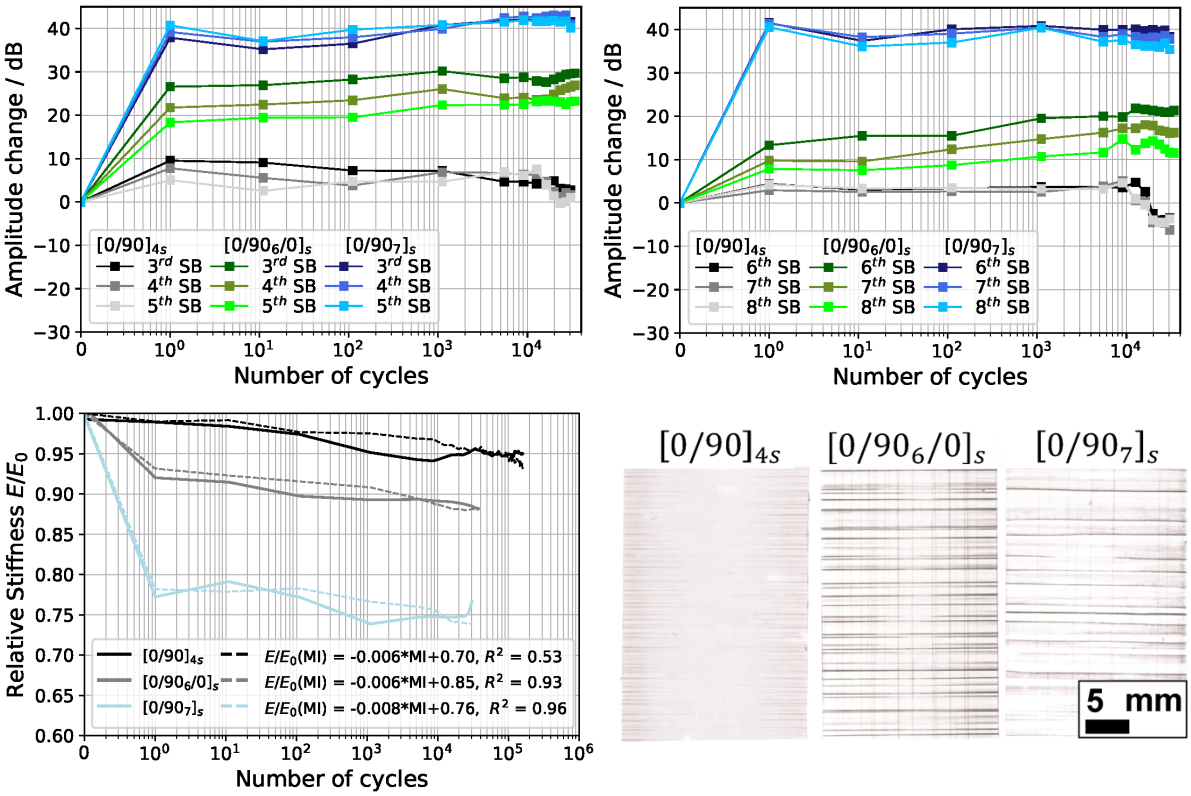

Figure 5: Representative results of fatigue tests on CP CFRP laminates with $[0/90_7]_s$, $[0/90_6/0]_s$ and $[0/90]_{4s}$ layup, including the amplitude change of 3rd-5th sidebands (upper left) and the 6th-8th sidebands (upper right) over the number of cycles tested at a stress ratio R=0.1. Correlation of the specimen stiffness E/E_0 on CP laminates with $[0/90_7]_s$, $[0/90_6/0]_s$ and $[0/90]_{4s}$ layup by using the MI (lower left). Corresponding x-ray scans after the respective cyclic loading are shown in the lower right section

The correlation between MI and specimen stiffness is shown in Figure 5 (lower left). In this context, the relative stiffness was reconstructed based on MI. The functions approximate the MI curves of the CP samples particularly well. In the case of $[0/90_7]_s$ and $[0/90_60]_s$ samples, R^2 is 0.93 and 0.96, respectively. However, the function also follows the stiffness curve for the $[0/90]_{4s}$ sample. With an R^2 of 0.53, the fit curve is not so well approximated, which might result from the stiffness decrease due to the fatigue cracks being relatively small and the MI not increasing much either.

In the $[0/90_7]_s$ laminate with the highest 90° layer thickness, the inter-fibre cracks can spread over 14 adjacent layers, resulting in cracks with a high cross sectional area. From the X-ray scans, the total amount of cracks decreases with increasing adjacent 90° layers, while conversely the amount of cracks running through the layer thickness and through the entire specimen width increases (see Figure 5 lower right). Consequently, a larger crack opening with high local strains by pump vibration generates a higher envelope amplitude and hence the highest modulation. As expected, reducing the number of adjacent 90° layers prevents the crack propagation and results in defects with a smaller cross-section. Therefore, these cracks have less stiffness-reducing effect, resulting in minimal modulation change but an increase in the number of cracks. In conclusion, vibro-acoustic modulation provides more sensitive results with regard to the crack size (in relation to the cross-sectional area of the pump wave propagation) compared to the crack density.

Quasi-isotropic laminates

As depicted in Figure 6, QI specimens with a high layer thickness (268 g/m^2) show a completely different vibro-acoustic behavior during tensile fatigue load compared to CP laminates. To analyse the damage state using a vibro-acoustic signal, different criteria were applied. Firstly, the signal was

analysed in the time and frequency domain. In this case, the response signal is shown representatively at 200 kHz in the time domain. Secondly, X-ray scans of the specimens were made at characteristic points of the stiffness condition. The linear sideband amplitude and MI increase is in very good agreement with the linear relative stiffness reduction until 4681 load cycles. The X-ray scan after 1111 cycles indicates that multiple inter-fibre fractures have developed in the $\pm 45°$ and 90° layers. Pronounced cracks are visible on the outside of the sample. With progressive fatigue loading, an exponential stiffness reduction accompanies it. In this phase, high interlaminar shear stresses occur at these inter-fibre fractures and lead to shear cracks, which develop into increasingly larger delaminations under fatigue load. Based on the X-ray image, it is evident that the delaminations spread from the edge of the sample, extending into the centre. These delaminations are located at the strongest stiffness gradient, between the 0° layers in the middle and the adjacent 45° layers.

Furthermore, the progressive separation of the individual layers leads to friction at the individual layers with the initiation of longitudinal oscillation. As a result, the vibro-acoustic response signal in the time domain is influenced by additional vibrations. It deviates from a pure sinusoidal envelope as seen with interfibre fractures to more complex oscillations in a sine-like shape. The increase of the interfaces due to the delaminations is an explanation for the decrease of carrier and sideband amplitude. The decrease of the carrier amplitude is stronger than the decrease of the first sideband, hence the MI increases. In addition, once the single layers are delaminated, the Lamb waves will not propagate within the entire specimen thickness, but only in the last contiguous layers at the surface of the piezoceramic. After the sample has passed through the exponentially decreasing stiffness range in which the first delaminations occurred, a relatively constant plateau follows in which the damage continues growing and a slight but continuous stiffness reduction becomes detectable until the final failure occurs. The increasing amount and propagation of delaminations is reflected in the X-ray scan and in the more pronounced deviation of the sinusoidal signal of the envelope in the time domain.

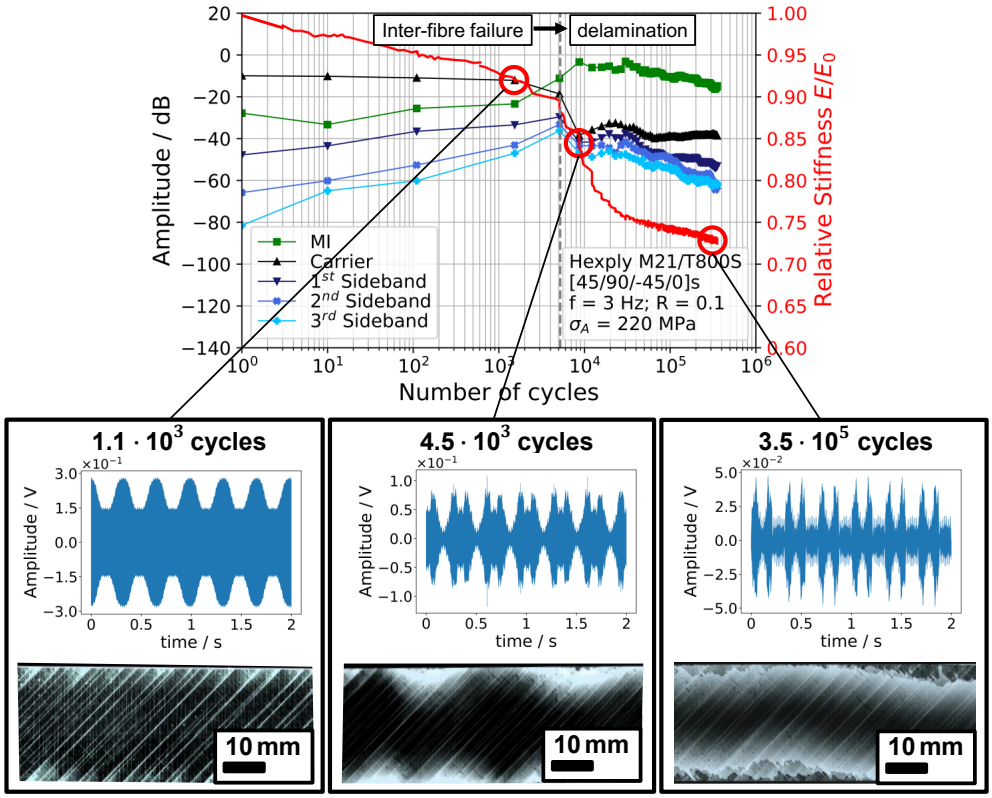

Figure 6: Representative results of fatigue tests on a quasi-isotropic laminate $[45/90/-45/0]_s$ with 268 g/m^2 - showing relative stiffness E/E_0, amplitudes of carrier, MI and first three sidebands over number of cycles tested with stress ratio R=0.1 and corresponding x-ray images for three specific damage states

Fatigue tests of thin-ply laminates [30, 60, 120 g/m2]

The results of the tension-tension fatigue tests of thin-ply laminates are shown in Figure 7. The diagramm on the left-hand side represents the relative reduction of the specimen stiffness with a fatigue stress amplitude of 220 MPa. The typical stiffness curve of QI fibre composite is observable in all laminates. The initial area where the number of inter-fibre breaks increases and propagates, resulting in a constant linear decrease in stiffness, sustains longer in the thin-ply laminates with 30 and 60 g/m^2. Among the thin-ply samples with 120 g/m^2 as well as the thick-ply samples with 268 g/m^2 the inter-fibre fractures result in delaminations, which can be identified by the pronounced decrease in the stiffness curve. With an increase of the fatigue amplitude to 275 MPa, even in the 60 g/m^2 samples some delaminations occur but the general damage behaviour is characterised by a brittle nature with intermediate fibre fractures dominating. This mechanical behaviour agrees very well with the vibro-acoustic measurement results. With regard to the samples with delamination-dominant behaviour (120 g/m^2 and 268 g/m^2 the sideband amplitudes increase until 44.2$\pm$2.3 dB for 268 g/m^2 respectively 35.1$\pm$1.4 dB for 120 g/m^2 with interfibre fractures occurrence. This shows a stronger increase in sideband amplitude with higher layer thickness and indicates an earlier onset of the increase. These findings are in good agreement with the results from the CP laminates, where the increase of sideband amplitudes is more pronounced with increasing crack size and length. However, the fatigue amplitude maximum, the threshold for delamination, is also reached earlier with higher layer thickness. This is well reflected in the relative stiffness curve. The reason for these mechanical results is analogous to the QI laminates with high layer thickness and characteristic for QI laminates with the occurrence of large-area delaminations. In contrast, for the specimens with inter-fibre failure-dominant damage behaviour, only an increase in sideband amplitudes is evident, which is less pronounced. The sideband amplitudes of the 30 g/m^2 sample with smaller crack size increases by 6.2 dB, while the 60 g/m^2 sample increases by 25.4 dB.

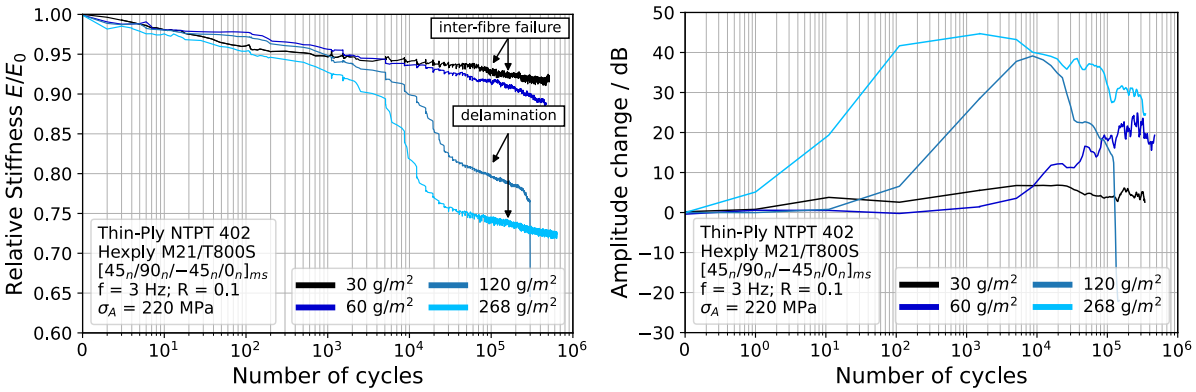

Figure 7: Fatigue results with relative reduction of the specimen stiffness E/E_0 (left) and change of (representative) 3rd sideband amplitude (right) on quasi-isotropic laminates with different fibre areal weight (30, 60, 120 and 268 g/m^2)

4 CONCLUSIONS

With the vibration-based NDT method presented in this paper, defects within CFRP and GFRP laminates can be monitored under static and fatigue load with different layups. The step-wise tensile tests confirmed the applicability of double-sided adhesive tape for attaching piezoceramic elements. A correlation exists between the stiffness decrease due to fatigue damage such as inter-fibre fractures and delaminations and the vibro-acoustic modulation. The crack size and crack density influence their magnitude and our results suggest that the changes in the VAM signal originate in the change of the global eigenfrequency of the structure due to a decreasing Young's modulus upon fatigue loading. Inter-fibre fractures, both in the 90° and in the 45° layers, lead to an increase in the sideband amplitudes as well as their amount, which is accompanied by a linear decrease in stiffness in log scale. It can be concluded that in this measurement method, the crack size has a more significant influence on the

characteristic values than the crack density. Nevertheless, even cracks with diameters of 0.1 to 0.3 mm in CP laminates can be detected by VAM. In contrast, large-scale, pronounced delaminations cause an abrupt stiffness-proportional decrease in the sideband amplitudes due to secondary vibrations caused by friction of the separated individual layers and the decrease in signal strength. With propagating delaminations, the envelope of the modulation deviates more and more from the pure sine, as the response signal in the time domain reveals. In addition, by correlating sideband amplitude with relative stiffness and identifying the effects of specific damage on sideband amplitude, critical cycling at selected stress amplitude can be recognised and a sideband threshold can be defined just before delamination occurs, allowing failure prediction. The results of the fatigue tests of the QI laminates with varying ply thickness have shown although the modulation is lower for brittle material behaviour with multiple inter-fibre fractures and small crack diameters. However, structural health monitoring is still possible even with 30 g/m^2 thinply laminates. The most successful failure prediction method for GFRP uses the MI's growth calculated after 1,000 load cycles for the predicted MI progression.

Compared to other continuous NDT methods, such as acoustic emission measurements or active pulsed Thermography on CFRP, the VAM measurement method enables damage detection even after it has occurred. The advantage of the VAM method is its ability provide both continuous and incremental measurements. Hence, the structural integrity of components could be variably verified by interval testing, as is done in aircraft inspections. The excitation of the low-frequency vibration using the servo-hydraulic testing machine is very effective and has worked very well for the vibro-acoustic measurement under laboratory conditions. However, an ideal sinusoidal vibration is produced, similar to most other VAM publications [17,19,24,25]. The existing ambient vibrations in practice, which could be used as low-frequency vibration, are super-positions of 10-20 Hz on bridges [19,26] and of low-frequencies (1-4 Hz) to over 500 Hz on wind turbines [27]. A challenge therefore arises in the use of the ambient vibration for the VAM measurement. Nevertheless, precise research into understanding VAM effects in fibre-reinforced polymers at laboratory level is essential before this use becomes possible. For larger components, whose size requires a sensor network consisting of several piezoceramics, a more complex test setup is necessary. Challenges include the energy consumption required for lamb wave excitation, the high sampling rate, the complex evaluation of the vibration data and its transmission. For this purpose, Oppermann et al. [19] have reduced the required amount of memory and computational resources for data evaluation significantly with the short-time Fourier-transform (STFT) on a strongly undersampled signal.

REFERENCES

[1] T. O'brien, Characterization of delamination onset and growth in a composite laminate, Damage in composite materials (1982) 140.

[2] S. Ogin, P. Smith, P. Beaumont, Matrix cracking and stiffness reduction during the fatigue of a (0/90)s gfrp laminate, Composites Science and Technology (1985) 23–31 doi:10.1016/0266-3538(85)90088-0.

[3] N. Kosmann, J. Karsten, M. Schuett, K. Schulte, B. Fiedler, Determining the effect of voids in GFRP on the damage behaviour under compression loading using acoustic emission, Composites Part B: Engineering 70 (2015) 184–188. doi:10.1016/j.compositesb.2014.11.010.

[4] A. Arteiro, C. Furtado, G. Catalanotti, P. Linde, P. P. Camanho, Thinply polymer composite materials: A review, Composites Part A: Applied Science and Manufacturing 132 (2020). doi:10.1016/j.compscitech.2014.06.027.

[5] S. Sihn, R. Y. Kim, K. Kawabe, S. W. Tsaic, Experimental studies of thin-ply laminated composites, Composites Science and Technology 67 (6) (2007) 996–1008. doi:10.1016/j.compscitech.2006.06.008.

[6] R. Amacher, J. Cugnoni, J. Botsis, L. Sorensen, W. Smith, C. Dransfeld, Thin ply composites: Experimental characterization and modeling of size-effects, Composites Science and Technology 101 (2014) 121–132. doi:10.1016/j.compscitech.2014.06.027.364

[7] J. Cugnoni, R. Amacher, S. Kohler, J. Brunner, E. Kramer, C. Dransfeld, W. Smith, K. Scobbie, L. Sorensen, J. Botsis, Towards aerospace grade thin-ply composites: Effect of ply thickness, fibre, matrix and interlayer toughening on strength and damage tolerance, Composites Science and Technology 168 (2018) 467–477. doi:10.1016/j.compscitech.2018.08.037.

[8] M. R. Wisnom, B. Khan, S. R. Hallett, Size effects in unnotched tensile strength of unidirectional and quasi-isotropic carbon/epoxy composites, Composite Structures 84 (2008) 21–28. doi:10.1016/j.compstruct.2007.06.002.

[9] C. Boller, Encyclopedia of Structural Health Monitoring, John Wiley & Sons, Ltd., 2009.
[10] R. Lammering, U. Gabbert, M. Sinapius, T. Schuster and P. Wierach, Lamb-Wave Based Structural Health Monitoring, Springer International Publishing, 2017.
[11] A. Klepka, L. Pieczonka, W. J. Staszewski, F. Aymerich, Impact damage detection in laminated composites by non-linear vibro-acoustic wave modulations, Composites Part B: Engineering 65 (2014) 99–108. doi:10.1016/j.compositesb.2013.11.003.
[12] L. Pieczonka, P. Ukowski, A. Klepka, W. J. Staszewski, T. Uhl, F. Aymerich, Impact damage detection in light composite sandwich panels using piezo-based nonlinear vibro-acoustic modulations, Smart Materials and Structures 23 (10) (2014). doi:10.1088/0964-1726/23/10/105021.
[13] F. Aymerich, W. J. Staszewski, Experimental study of impact-damage detection in composite laminates using a cross-modulation vibro-acoustic technique, Structural Health Monitoring 9 (6) (2010) 541–553. doi:10.1177/1475921710365433.
[14] H. J. Lim, H. Sohn, Online fatigue crack prognosis using nonlinear ultrasonic modulation, Structural Health Monitoring 18 (5-6) (2017) 1889–1902. doi:10.1177/1475921719828271.
[15] D. M. Donskoy, A. M. Sutin, A. E. Ekimov, Nonlinear acoustic interaction on contact interfaces and its use for nondestructive testing, NDT & E International 34 (4) (2001) 231–238. doi:10.1016/S0963-8695(00)00063-3.
[16] L. Pieczonka, A. Klepka, A. Martowicz, W. J. Staszewski, Nonlinear vibroacoustic wave modulations for structural damage detection: an overview, Optical Engineering 55 (1) (2015) 011005. doi:10.1117/1.oe.55.1.011005.
[17] L. Dorendorf, N. Lalkovski, M. Rutner, Physical explanation for vibro-acoustic modulation due to local and global nonlinearities in a structure and its experimental and numerical validation, Journal of Sound and Vibration 528 (2022). doi:10.1016/j.jsv.2022.116885.
[18] D. M. Donskoy, M. Ramezani, Separation of amplitude and frequency modulations in vibro-acoustic modulation nondestructive testing method, Proceedings of Meetings on Acoustics 34 (1) (2018). doi:10.1121/2.0000831.
[19] P. Oppermann, L. Dorendorf, M. Rutner, C. Renner, Nonlinear modulation with low-power sensor networks using undersampling, Structural Health Monitoring (2021). doi:10.1177/1475921720982885.
[20] M. Ramezani, E. Stevens Institute of Technology. Department of Civil, O. Engineering, Enhancement of Joining Method and Damage Detection Methodology in Structural Materials, Stevens Institute of Technology,2018.
[21] H. Hu, W. Staszewski, N. Hu, R. Jenal, G. Qin, Crack detection using nonlinear acoustics and piezoceramic transducers—instantaneous amplitude and frequency analysis, Smart Materials and Structures 19 (6) (2010). doi:10.1088/0964-1726/19/6/065017.
[22] P. Oppermann, L. Dorendorf, B. Boll, A. Gagani, N. Lalkovski, C. Renner, M. Rutner, R. Meißner, B. Fiedler, Towards structural health monitoring using vibro-acoustic modulation in the real world, in: 18. GI/ITG KuVS FachGespräch SensorNetze, FGSN 19-20.9. 2019, Magdeburg, 2019, pp. 21–24. doi:10.25673/28428.
[23] ASTM 3039:00-, Standard test method for tensile properties of polymer matrix composite materials, 2000
[24] D. M. Donskoy, Nonlinear acoustic interaction on contact interfaces and its use for nondestructive testing, Encyclopedia of Structural Health Monitoring (2009). doi:10.1002/9780470061626.shm014.
[25] B. Boll, E. Willmann, B. Fiedler, R. Meißner, Weak adhesion detection – enhancing the analysis of vibroacoustic modulation by machine learning, Composite Structures 273 (2021). doi:10.1016/j.compstruct.2021.114233.
[26] K. Smarsly, M. Worm, K. Dragos, J. Peralta Abadia, M. Wenner, O. Hahn, Mobile structural health monitoring using quadruped robots, Health Monitoring of Structural and Biological Systems XVI,SPIE 12048 (2022) 404–417. doi:10.1049/iet-rpg.2013.0229.
[27] C. J. Doolan, D. J. Moreau, L. A. Brooks, Wind turbine noise mechanisms and some concepts for its control, Acoustics Australia 40 (2012)